ANALYSIS OF THE MECHANICS OF PREFORATION BY PROJECTILES

G. Liaghat

Department of Mechanical Engineering
Tarbiat Modarres University
Tehran, Iran

ABSTRACT To explain the mechanics of perforation of thick metallic target plates a modified version of the analysis suggested by Awerbuch and Bodner [2] is given by a cylindrical projectile. Although the analysis retains the basic concept of the perforation process to occur in three stages as was assumed by Awerbuch and Bodner [2], a new explanation, as to the cause and effect of the compressive force is suggested. Attention is also drawn to the force required to cause internal plastic deformation of the target material, during the passage of the projectile. In addition, the mass of the target material ahead of the projectile is modified in the manner of Tate [17]. The analysis retains the initial entrance diameter to be the same as that of the projectile, at the instant the projectile hits the target and assumes that the final length of the plug is attained at the end of the process instead of at the beginning of the second stage. The computed results using the modified analysis yield better agreement with the experiments for the perforation process especially for plates whose thicknesses are between 1 and 2.5 times the projectile diameter.

چکیده در این مقاله مدل ریاضی مکانیک نفوذ گلوله در هدفهای ضخیم فلزی که توسط آوربوخ و بودنر (۲) بیان شده بود، اصلاح و بصورت مدل بهتری ارائه گردیده است. علاوه بر تغییرات در شکل هندسی اولیّه مدل، توضیح جدیدی از وجود و اثرات نیروی فشاری (FC) و همچنین تغییر شکلهای داخلی در هدف ناشی از حرکت گلوله و ایجاد نیروی پلاستیکی داخلی (FPD) و نیز نیروی اینرسی مخالفت کننده در مقابل حرکت گلوله (FI) بیان گردیده است. مقدار ماده هدف که بعد از برخورد گلوله با آن به حرت درمی آید نیز تابعی از مشخصات هندسی لحظه ای گلوله فرض گردیده و نحوه محاسبه آن نیز اصلاح شده است. قطر سوراخ ورودی اولیه در هدف را برابر با قطر گلوله در لحظه برخورد (Do) و تغییرات لحظه ای سوراخ ایجاد شده در آن فرض شده است. نتایج تئوریک بدست آمده از مدل ارائه شده در این مقاله بسیار نزدیک به نتایج آزمایشات بوده و مخصوصاً برای هدفهائی که ضخامت آنها بین ۱ تا ۲/۵ برابر قطر گلوله هستند نتایج بهتری را در مقایسه با تئوری های منابع (به منابع آخر مقاله رجوع شود) ارائه می دهد.

INTRODUCTION

The theoretical modeling of high speed perforation of a target plate by a cylindrical projectile is a complex problem. Various theories have, however, been proposed to explain the salient features of the process. Perforation may occur with different modes of deformations depending on the relative size, geometry and thickness of the plate vis-a-vis that of the projectile. Among these deformation modes are: shearing of a plug, ductile hole enlargement and the dishing of the target material[1]. Previous theoretical approaches to the problem have been concerned with using either the energy balance method or the momentum balance method as can be found for example, in the works of Taylor [4] and Thomson [5] and that of Zaid and Paul [6,7,8]. Besides these many other investigations such as those given in references [10-17], have advanced solutions of the problem employing one or other of these methods.

Ravid and Bodner [18] have recently attacked the problem using the modified upper bound theorem of plasticity. Liss, et al. [19] and Yuan Wenxue et al. [20] have also recently given a somewhat novel perforation analysis employing plastic wave theory.

Of the various analyses mentioned above the one suggested by Awerbuch and Bodner [2] is very instructive. It provides an approach based on a simple mathematical model which yields reasonably good results for the perforation

process. The analyses given in reference [2] are a development of the preliminary work performed by Awerbuch [14] and expanded by Goldsmith and Finnigan [15]. The more recent work by Ravid and Bodner [18] uses an upper bound approach to the flow model, modified to include dynamic effects. The model has the capability to predict the residual velocity of the projectile, the size of the plug and of the bulge shape.

The present investigation provides a modification of the analysis given in reference [2]. Here, besides putting forward a new explanation for the cause and effect of the compressive force Fc exerted on the penetrator which is assumed to act in the first and second stages of the penetration process, an additional force F_{PD} is introduced. This is the component of the force exerted by the projectile as it does plastic work required to cause plastic deformation within the target material.

Since the shearing force is also included in the concept of F_{PD}, the shearing force F_s appearing in [2], at the stage appropriate to this force is neglected. The calculations give results which are not only more accurate for the residual velocity but also, in some cases, estimate the total duration of the perforation process more accurately.

MECHANICS OF PROJECTILE PENETRATION

To establish the present modified analysis, a brief summary of the salient points of the analysis given in [2] is presented here.

1. Existing Model and Formulation

The basic model for the perforation process proposed by Awerbuch and Bodner consists of three distinct stages. With reference to Figure 1 these stages are as follows:

Stage I: Initial compression of plate material in front of the projectile with no shearing at the periphery.

Stage II: Penetration of the plug through the remaining plate material.

Stage III: Shearing of the full plug from the plate after the final growth of the plug.

2. Present Analysis

The following assumptions are made in the present analysis:

i) There is no bending of the target plate. Although in practice it is observed that some bending may happen near the ballistic limit velocity.

ii) The target material is incompressible and flows irrotationally.

iii) Although the penetration is fast, the projectile has time to slow down due to the resistance offered by the target material. On the contrary, that part of the target material which forms the plug has enough time to accelerate in such a way that its velocity increases to the final velocity of the plug.

iv) There is only a small radial expansion of the target around the projectile path and this corresponds to the expansion of the plug in front of the projectile.

v) The effect of stress wave is neglected.

The modifications and additions of the present analysis are as follows:

1) The basic geometry of the penetration model is changed to that shown schematically in Figures 2(a) - 2(d). This is done to include the effect of progressive changes in the geometry of the plug on the existing force.

2) At the beginning of Stage I, the projectile retains its original diameter. During the process, the projectile diameter increases because of its deformation.

3) The added mass appearing in the momentum equation in the analysis given in reference [2] is changed to the mass of the target material displaced by the projectile nose in contact with the target in a manner similar to that suggested by Tate [17]. Although Tate considers the added mass for Stage I, in the present analysis, it is extended to both Stages I and II.

4) The compressive force Fc developed in the target plate during Stages I and II, has a value of $2\sigma_y A$ used instead of $\sigma_c A$, as used in [2]. The basic explanation for this alteration is given in the text.

5) An additional force denoted by F_{PD}, required for internal plastic deformation and shearing, is added to the other forces acting on the projectile in both Stages I and II. The other forces acting are F_I and F_C, the inertial and compresive forces, respectively. To evaluate force F_{PD}, it is assumed that the target material deforms as a rigid-perfectly plastic material.

(6) With the addition of the force F_{PD}, since it contains the shear force, the shearing force F_S, occuring separately is excluded in Stage II.

(7) The length of the plug C, at the end of the process is taken to be less than its length at the begining of second stage C_2.

Estimation of Internal Plastic Deformation Force 'F_{PD}'

At the beginning of the perforation process only a small amount of the target material is pushed forward. This will not show up at the bottom of the plate, but will probably cause the diameter of the projectile to increase in expense of decreasing its length. As the projectile advances, the tangent material in front of it (plug) deforms plastically and shifts forward. Some of this deformation ends up on the other side of target plate, while the diamter of the hole made in the target plate increases due to the deformation of plug. To calculate the force required for plastic deformation of the target material, F_{PD}, tangential velocity discontinuity patterns, Figures 3(a) and 4(a) are assumed which are consistent with the axial deformation of the target material, due to the movement of the projectile. The hodographs for these two kinematically admissible, tangential velocity discontinuity patterns are shown in Figures 3(b) and 4(b), respectively.

An estimation of the rate of plastic work done by the yield shear stress k, on the material as it crosses each of the velocity discontinuity surfaces is produced following the procedure given by Adie and Alexander [21]. Summing up the rates of plastic work expended across these velocity discontinuity surfaces and equating the result to rate of work done by the force F_{PD}, the plastic force may be estimated. With reference to Figures 3(a), 3(b), and 4(a), 4(b) the rate of energy dissipation in crossing the tangential velocity discontinuities for the axi-symmetric flow may be written as.

$$\dot{\omega} = \int_s k\, W_s\, ds, \qquad (1)$$

Where W_S is tangential shear velocity and S is the surface area. For each stage of the perforation process the rate of plastic work done by the projectile in pushing the target material over each of the discontinuity surfaces may thus be obtained and summed up.

For the kinetically admissible velocity field shown in Figure 3(a) and the corresponding hodograph Figure 3(b) for Stage I and for Figures 4(a) and 4(b), for Stage II, the total rate of energy dissipation is,

$$\dot{\omega}_{ic} = \pi k_c a_{ic}^2 W_{ic}(x) \left[\frac{\sin\beta_{ic}}{\sin\alpha_{ic}\sin(\pi-\alpha_{ic}-\beta_{ic})} + \frac{\sin\beta_{ic}}{\sin\alpha_{ic}\sin(\alpha_{ic}-\beta_{ic})} + \frac{[b_{ic}^2-a_{ic}^2]\sin(\pi-\alpha_{ic})}{b_{ic}^2\sin\beta_{ic}\sin(\alpha_{ic}-\beta_{ic})} \right] \qquad (2)$$

where i = 1, 2 for Stages I and II and the subscript c refers to current, updated values of the parameters corresponding to each small advancement of the projectile. The current value of the force F_{PD} at each small increment of the pentetrant is given as,

$$F_{PDic} = \pi k_c a_{ic}^2 \left[\frac{\sin\beta_{ic}}{\sin\alpha_{ic}\sin[\pi-\alpha_{ic}-\beta_{ic}]} + \frac{\sin\beta_{ic}}{\sin\alpha_{ic}\sin[\alpha_{ic}-\beta_{ic}]} + \frac{[b_{ic}^2-a_{ic}^2]\sin[\pi-\alpha_{ic}]}{b_{ic}^2\sin\beta_{ic}\sin[\alpha_{ic}-\beta_{ic}]} \right] \qquad (3)$$

Where, a, b, α, β, etc., are as shown in Figures 3 and 4, h, is the target thickness and x the instantaneous depth of the projectile and k_C is the current dynanic shear stress.

Considering the strain rate effects, the shear stress k in the above equation is taken in the Bingham form as $k = k_O + \mu \dot{Y}$ where, μ is the coefficient of viscosity and $\dot{Y}$ is the shear strain rate ($= W/e$). Here e is the radial width of the shear zone of the target material and is estimated experimentally, (see ref [2]).

Estimation of the Compressive Force, F_C

The compressive force FC, is assumed to be uniformly distributed over the projectile nose and is taken to be

$$F_c = \sigma_z A \qquad (4)$$

Where σ_z is the axial stress and A the projected area of the projectile nose.

To determine σ_z and therefore, the compressive force, we may proceed in either one of the two following ways:

(a) That the compressive force acting on the target material immediately underneath i.e. plug, causes the target surface surrounding the plug to become fully plastic and this plastic zone spreads to some distance away from the axis of the plug.

(b) That there is assumed a sufficient layer at the bottom of the target plate (reasonable because of the high speed of the process) and the compressive force is resisted by the surrounding plate material in such a way that any radial expansion caused to the material beneath i.e., plug, is brought back by the surrounding elastic material which does not allow the plug to be pushed sideways.

For target plates of thicknesses lying between two entrances 1mm and 19mm used during the course of experimental investigation, the results given by each of the two modes will vary. The one which yields the least value of the compressive force is probably the most likely mode of deformation. In the method of interpretation used for the penetration problem a detailed analysis has been made.

The results for the compressive stress σ_z were observed to vary between $1.84\ \sigma_y$ - $2.1\ \sigma_y$, where σ_y is the yield stress of the material. It will therefore be quite reasonable to assume $\sigma_z = 2.0\ \sigma_y$ and the resultant compressive force to be expressed approximatley as,

$$F_c = 2\ \sigma_y\ A \qquad (4a)$$

Modification to the Added Mass Ahead of the Projectile

The equation of motion for the penetration process may be written

$$\frac{d}{dt}(MW) = -F \qquad (5)$$

where, M is the mass, W the current velocity and F the total force acting on the projectile.

According to Tate [17] the lefthand side of equation (5) can be written as,

$$M\frac{dW}{dt} = -F \qquad (6)$$

Where

$$M = M_o + \rho A C' \qquad (7)$$

π is the density of the target, c' is a constant on the projectile surface and can be determined from the potential flow ahead of the projectile. M_O is the initial mass of the projectile. According to Tate, $C' = r/4$, and the general equation of motion will be of the form,

$$(M_o + \rho A r/4)\frac{dW}{dt} = -F = -[F_{PD} + F_I + F_C] \qquad (8)$$

(r is taken as the maximum radius of the crater at each stage and F_I is the inertial force acting on the projectile.

3. Mechanics of Projectile Penetration with the New Formulation

Stage: The equation of motion for the first stage of the process is written as,

$$\left[M_o + \frac{PA_1 b_1}{4}\right]\frac{dW_1(X)}{dt^1} = -[F_{PD1} + F_{I1} + F_{C1}]$$

$$= -F_1 \qquad (9)$$

Considering the new geometry Figures 2(a) -2(d), for the first stage of the perforation process, the forces F_I, F_C and F_{PD} act on the projectile and can be written as,

a) Inertial Force $F_{I_{1c}}$

Using the same analysis as [2] we can obtain the inertial force as,

$$F_{I1c}=\tfrac{1}{2}K\rho A_{ic}W_{ic}^2 \qquad (10)$$

where K is the projectile nose shape factor.

b) Compressive Force $F_{C_{1c}}$

$$F_{C1c}=2\sigma_y A_{1c} \qquad (11)$$

c) Force required for internal plastic deformation $F_{PD_{1c}}$

Referring to Figures 3(a) and 3(b), this force is expressed as,

$$F_{PD1c}=\pi a_{1c}^2\left[k_o+\mu\frac{W_{1c}}{e}\right]\left[\frac{\sin\beta_{1c}}{\sin\alpha_{1c}\sin[\pi-\alpha_{1c}-\beta_{1c}]}+\frac{\sin\beta_{1c}}{\sin\alpha_{1c}\sin[\alpha_{1c}-\beta_{1c}]}+\frac{[b_{1c}^2-a_{1c}^2]\sin[\pi-\alpha_{1c}]}{b_{1c}^2\sin\beta_{1c}\sin[\alpha_{1c}-\beta_{1c}]}\right] \qquad (12)$$

Substituting equations (15), (16) and (17) into (14) and performing the necessary mathematical operation, lead to

$$\frac{dW_1(x)}{dx}=\left\{\pi a_{1c}^2\left[k_o+\mu\frac{W_{1c}}{e}\right]\left[\frac{\sin\beta_{1c}}{\sin\alpha_{1c}\sin[\pi-\alpha_{1c}-\beta_{1c}]}+\frac{\sin\beta_{1c}}{\sin\alpha_{1c}\sin[\alpha_{1c}-\beta_{1c}]}+\frac{[b_{1c}^2-a_{1c}^2]\sin[\pi-\alpha_{1c}]}{b_{1c}^2\sin\beta_{1c}\sin[\alpha_{1c}-\beta_{1c}]}\right]+\tfrac{1}{2}K\rho A_{1c}W_{1c}^2+2\sigma_y A_{1c}\right\}\Big/\left[M_o+\frac{\rho A_{1c}b_{1c}}{4}\right]W_{1c} \qquad (13)$$

Where $W_1(x)$, is the current velocity of the projectile during the first stage and is calculated numerically using a computer subroutine based on equation (19). From this, an instantaneous force acting on the projectile is also obtained by summing the current values of the three forces F_{I_c}, F_{C_c}, and F_{PD_c}.

The time required for the projectile to penetrate a distance x, (see Figure 2) was calculated by integrating the expression

$$t_1=\int_s^x\frac{dx}{W_1(x)} \qquad (14)$$

Stage II: This stage of the perforation process begins when the compressive force Fc_2 starts decreasing. The length of the plug at the beginning of this stage is obtained by considering the assumed geometry and the assuption of volume constency of the material. If r_B r_C, r_D, and r_E refer to the radii of the plug at the points shown in Figure 1 and equating the volume of the plug at the beginning of second stage to the volume of it at the end of process, (see Figure 1), we have

$$\tfrac{1}{3}\pi C_2[r_B^2+r_Br_C+r_C^2]=\tfrac{1}{3}\pi C[r_D^2+r_Dr_E+r_E^2]$$

or $C_2[r_D^2+r_Dr_E+r_E^2][r_B^2+r_Br_C+r_C^2]$

Here C_2 and C are the lengths of the plug at the beginning of the second stage and at the end of the process, respectively.

The equation of the motion for the second stage of the perforation process is written as,

$$\left[M_o+\frac{PA_2b_2}{}\right]\frac{dW_2(X)}{}=-[F_{PD_2}+F_{I_2}+F_{C_2}]=-F_2 \qquad (15)$$

The force component F_{PD_2}, F_{I_2} and F_{C_2} can be obtained in the same way as in Stage one.

These are written as,

a) Inertial force

$$F_{I_{2c}}=\tfrac{1}{2}K\rho A_{2c}W_{2c}^2 \qquad (16)$$

b) Compressive force $F_{C_{2c}}$. This force is equal to zero at the end of this stage, where x = h. Therefore, the equation for F which meets the

limiting condition, is expressed as,

$$F_{C2c} = 2\sigma_y A_{2c} \left\{ \left[\frac{x-(h-C^2)}{C_2} \right]^2 \right\} \quad (17)$$

c) Force required for internal plastic deformation $F_{PD_{2c}}$.

Referring to the earlier discussion, the F_{PD} acting on the projectile at each instant in the second stage is expressed as,

$$F_{PD2c} = \pi a_{2c}^2 \left[k_o + \mu \frac{W_{2c}}{e} \right] \left[\frac{\sin\beta_{2c}}{\sin\alpha_{2c}\sin[\pi-\alpha_{2c}-\beta_{2c}]} + \frac{\sin\beta_{2c}}{\sin\alpha_{2c}\sin[\alpha_{2c}-\beta_{1c}]} + \frac{[b_{2c}^2-a_{2c}^2]\sin[\pi-\alpha_{21c}]}{b_{2c}^2\sin\beta_{2c}\sin[\alpha_{2c}-\beta_{2c}]} \right] \quad (18)$$

The equation of motion for the second stage therefore is,

$$\frac{dW_2(x)}{dx} = -\left\{ \pi a_{2c} \left[k_o + \mu \frac{W_{2c}}{e} \right] \left[\frac{\sin\beta_{2c}}{\sin\alpha_{2c}\sin[\pi-\alpha_{2c}-\beta_{2c}]} + \frac{\sin\beta_{2c}}{\sin\alpha_{2c}\sin[\alpha_{2c}-\beta_{2c}]} + \frac{[b_{2c}^2-a_{2c}^2]\sin[\pi-\alpha_{2c}]}{b_{2c}^2\sin\beta_{2c}\sin[\alpha_{2c}-\beta_{2c}]} \right] + \tfrac{1}{2}K\rho A_{2c}W_{2c}^2 + 2\sigma_y A_{2c} \left[1 - \left[\frac{x-(h-C^2)}{C_2} \right]^2 \right] \right\} / [M_o + \rho A_{2c} b_{2c}/4] W_{2c} \quad (19)$$

where a and b are the current top and bottom radii of the plug,

$W_2(x)$, the current velocity of the projectile in the second stage, was computed numerically from equation (19) and the total instantaneous force F_2 was obtained by simply adding together the above mentioned forces acting on the projectile at each instant during this stage.

The time required for the projectile to reach the rear surface of the target plate, (x=h) from the end of the first stage, ($x = h - c_2$) was calculated from

$$t_2 = \int_{x=h-C_2}^{x=h} \frac{dx}{W_2(x)}$$

Stage III: The third stage starts when the whole plug moves together with the projectile at the same velocity, (see Figure 2(d)). This stage is similar to that described in reference [2] with the only difference in calculating A_P, the circumferential area of the plug used, which is different because of the difference in the assumed geometry. During this stage, only the shear force $F_S = F_3$ acts over the surface of the plug. The equation of motion for the third stage is therefore

$$m_3 \frac{d^2z}{dt^2} = F_3 = -\tau A_P \quad (21)$$

where m_3 is the mass of the projectile and of the plug, τ is equal to $(\tau_O + \mu \frac{W}{e})$, F_3 is the shear force acting on the projectile, Z is the additional distance moved by the plug, as shown in Figure 2(d). Considering the new geometry assumed in this investigation, A_P, the curved surface area of the plug is given by,

$$A_P = \pi \left[\frac{D_E+D_D}{2} \right] \left\{ \left[\frac{D_E+D_D}{2} \right]^2 + C^2 \right\}^{\frac{1}{2}}$$

where D_D and D_E are the top and bottom diameters of the plug at the end of the second stage.

Equation (21) is written as,

$$\dot{Z} + \frac{A_P\mu}{m_3 e}\dot{Z} = \frac{\tau_o A_e}{m_3} \quad (23)$$

Equation (23) can be solved for $\dot{Z}$ and Z to give,

$$Z = \left[\overline{W}_2 + \frac{\tau_o e}{\mu} \right] \left[\exp\left[\frac{A_P\mu}{m_3 e} t_3 \right] \right] \frac{\tau_o e}{\mu} \quad (24)$$

and

$$Z=\left[\overline{W}_2+\frac{\tau_o e}{\mu}\right]\left[\exp\left[\frac{A_p\mu}{m_{3e}}t_3\right]\right]-\frac{\tau_o e}{\mu}t_3 \quad (25)$$

where, $\overline{W}_2$ is the velocity at the end of the sceond stage when t_3 = O. The time duration t_3, of the third stage is the time required for the material failure to occur. This occurs at a displacement $Z = Z_f = \Upsilon_f e$ [2], where Υ_f is the dynamic ultimate shear strain. The total duration time for the perforation process therefore is

$$t_f=t_1+t_2+t_3+t_p \quad (26)$$

where, t_P is the time required for the plug to leave the target plate and is equal to [2],

$$t_D=\frac{C-Z_1}{W_f} \quad (27)$$

where, W_f is the final (exit) velocity of the projectile.

RESULTS AND DISCUSSION

As mentioned before Awerbuch and Bodner [3] gave results of an extensive series of plate perforation experiments using lead and armour piercing bullets perforating different thicknesses of steel and aluminium plates. Projectile diameters of 5.6, 7.62 and 9 mm with projectiles identified by symbols T.T.R. - S.A.R.- S.A - A.R. with initial velocities in the range of 385 to 855 ms^{-1} were used. Plates of two different types of aluminium 1100- H14, and 6061- T6 with thickness between 1 and 19 mm and four different steel plates with thicknesses 6 to 12 mm were used in their penetration tests. The type and geometrical data of the projectiles and also the mechanical properties of the target plates are tabulated in Tables 1 and 2 of their paper.

The perforation mechanisms proposed by Awerbuch and Bodner [2] showed satisfactory agreement especially in case of thinner plates when compared with the experimental work reported in reference [3]. However, for thicker plates, the predicted results for the final velocities of the projectiles were much lower (25% - 44%) than those measured experimentally (e.g. Table 3 Tests n 1, 2, 3, 4, 6, 9, 10 of reference [13]). It was also stated in reference [3] that "The argeement is not so good for the other projeciles (S.A.P - S.R.) and for the steel alloy target plates where the calculated final velocities are about 15-25% lower than the experimental measurements".

In this paper details of the computed results for the residual final velocity and of the duration time, using the analysis above, are given in Table 1. All of the computed results are compared with the experimental values of the residual velocities and duration time as given by Awerbuch and Bodner [13], Wenxue et al. [20] and with three of the typical results (test no 11, 12, 13) given by Ravid and Bodner [18]. From Table 1, it may be seen that a much better agreement exists between the experimental values for the residual velocity and those calculated here.

One of the main difference between the analysis given in reference [2] and in this paper is in the geometrical consideration of the model. Considering Figures 2(a)-(d), although the basic concept of the perforation process as explained in [2] was retained, the geometry of the model has been changed. From the very beginning of the process, at the time of the first contact between the projectile and the target, the initial projected area of the projectile is taken as the area of the interface between the projectile and the target. Where in the case of Awerbuck and Bodner [2], this initial contact area is equal to the final entrance area of the hole in the target after-the end of the perforation process. This only increases as the process continues. Therefore, the entrance diameter of the cavity at the very beginning of the first stage is taken to be equal to the diameter of the projectile. Accordingly the diameter of the cavity in the target at different stages is chosen so as to conform to the condition that the final entrance

and exit diamters are D_1 and D_3, respectively. This is easily accommodated as may be seen in Figures 2(a)-(d). For the first stage, the entrance diamter of the cavity is taken to be equal to the initial diamter of the projectile D=2R. The exit diamater D_A in the first stage is assumed to be the average of 2R and the final entrace diameter of the hole in the target D_1=2a. The diameter D_1 is determined experimentally. For the second stage, the entrance diameter D_B is taken to be the average of the entrance and the exit diameters in the first stage and the exit diameter D_E is assumed as the average of the final exit diameter D_3=2b and D_D. the diameter D_D is taken to be $(D_B + D_C)$ /2 where, D_C is equal to $(D_B + D_2)/2$ and D_2 is the average of D_1 and D_3. As explained earlier, the length of the plug is considered to decrease until the end of the second stage where its final length is C. The length of plug at the end of first stage (beginning of second stage) C_2 is calculated from the geometry and from the volume constantancy. Where, in the case of Awerbuch and Bodner [2] C_2=C. D_1, D_3, C the length of the plug and e the width of the shear zone are however, determined experimentally and the viscosity of the rarget at high strain rate and, m is also considered an experimentally determined property.

In the case of thick targets, a discrepancy exists between the computed and experimental results using the analysis given in [2]. A major reason for this is due to the assumption of a large quantity of piled-up mass ahead of the projectile when it penetrates to a depth of more than one fourth the current cavity radius. This assumption does not have much effect on the computed residual velocity in the case of thin plates, because of the small amount of the target mass in front of the projectile, but it has a very substantial effect on the perforation of thick plates. In the present analysis the above anomaly has been corrected to a large extent, as explained earlier in the analysis for the added mass ahead of the projectile. Using this, it is no longer necessary to assume a piled-up mass ahead of the projectile as was done in reference [2].

The force "F_{PD}" in the first and second stages takes into account the work done against the internal shearing of the material. With reference to Figures 3(a) and 4(a), considering the discontinuous velocity pattern shown, the velocity discontinuties are along AP, PB, PC and PD. As the material above APB moves downwards and the particles cross PB, their directions of motion are instantaneously altered and these proceed parallel to BC; at PC, the velocity of each of the particles is instantaneously altered again and it proceeds along the same direction as the projectile movement. These criss-cross movements of the material necessitates some absorption of energy from the original velocity of the projectile and thus decreases its velocity. F_s which is the shearing force assumed in the analysis of [2] does not appear here, because by considering the work done against shear on the surface BC and including it in 'F_{PD}' takes account of the shearing force F_S as well.

The resisting compressive force in this analysis is taken as $2\sigma_y$ A, instead of σ_cA. In the past, it is found that σ_y approaches σ_c the ultimate stress at high strain rates and the reported results by many investigators show that the dynamic yield stress reaches a value 2-3 times its value in the static conditions. The magnitude of this fact appears to be material dependent. For perforation studies F_C may be based on a maximum value of 2.7 σ_y. [16]. It is therefore, justifiable to assume F_C as $2\sigma_y$ A, since for most of the metallic materials $\sigma_c < 2\sigma_y < 2.7\ \sigma_y$.

Typical sets of the computer results for test numbers 1, 12 and 30 listed in Table 1 are shown in the graphical form in Figures 5, 6 and 7, respectively. The figures show the variations in the depth of penetration of the projectile, in velocity and the total force with respect to time for all the three stages in each case. These graphs were plotted for the case of a standard regular lead bullet (S.R.) impacting a 6 mm steel target, a standard armour-piercing (S.A.P.)

projectile penetrating a 6.35 mm steel target and a 9 mm caliber lead bullet (A.R.) perforating a 6/35 mm thick aluminium alloy target, respectively. Figures 5(b) and 6(b) and 7(b) show the force-time relations for each of the force components F_{PD}, F_I, F_C for the three perforation stages: I, II and III. It may be seen from these figures, that the compressive force is increasing in Stage I due to the increase in area of cross-section of the projectile. The force for internal plastic deformation F_{PD} and inertial force F_I in Stage I are also increasing. The inertial force F_I and the compressive force F_C both decrease in the second stage. The compression force F_C becomes zero at the end of the second stage to satisfy the earlier assumption of having no F_C in the third stage. The only active force at the last stage is the shearing force F_S.

CONCLUSIONS

By retaining the basic concept in analyzing the mechanics of the perforation process in ballistic impact to occur in three stages as in reference [2], but some modifications to

a) the change in geometry

b) the change in formulation of the compressive force

c) the introduction of a new force 'F_{PD}' and

d) the introduction of a new length of the plug at the beginning of second stage and

e) incorporating the suggestion of Tate [17] regarding the amount of the added mass in front of the projectile lead to the present analysis. This yields a much better agreement with the experimental results for the final velocity and in most cases for the duration time especially for thick plates whose thicknesses are between 1 and 2.5 times the projectile diameter. The need for the same empirical parameters however, (as in reference [2]) still exits.

REFERENCES

1. M. Backman and W. Goldsmith, *Inst. J. Engng.* 16, 1 (1978).
2. J. Awerbuch and S.R. Bodner, *Into J, solid Structures* 10, 671 (1974).
3). J. Awerbuch and S. R. Borern, *Into J. Solid & Structure* 10, 685, (1974).
4. G.T. Taylor,*Quart. J, Mech. App. Math. 1, (1948)*
5. *W. T. Thompson. J. App. Phys.*, 26, 1 (1955).
6. M. Zaid and B. Paul, *J. Franklin Inst.* 264, 117 (1957).
7. B. Paul and M. Zaid, *J. Franklin. Inst.* 265, 317 (1958).
8. M. Zaid and B. paul, *J. Franklin Inst.* 268, 24 (1959).
9. A.V.Masket, *J. App. phys.* 20, 2, (1949).
10. J. Nishiwaki, *J. Phy. Soc. Japan*, 6, (1951).
11. W. Goldsmith, "Impact-The Theory of physical Behaviour of Colliding Solids", Edward Arnold Ltd. London (1960).
12. R.F. Recht and T.W. Ipson. *J. App. Mech.* 30 (1963).
13. V. Kucher, "Penetration with Optimal Work", Report No. 1384, Ballistic Research Lab. (1967).
14. J. Awerbuch, *Is J. Tech.* 8, 375 (1970).
15. W. Goldsmith and S. A. Finnegan, *Int. J. Mech. Soc.* 13, 843 (1971).
16. R.L.Woodward and M.E. Morton, *Int. J. Mech. Sci.* 18, 119 (1976).
17. A. Tate, *Int. J. Engng. Sci* 17, 341 (1979).
18. M. Ravid and S.R. Bodner, *Int. J. Engng. Sci* 21, 577 (1983).
19. J. Liss, W. Goldsmith and J. M. Kelly, *Int. J. Impact Engng.* 1, 321 (1983).
20. Y. Wenxue, z. Lanting, M. Xiaoging and W.J. Stronge, *Int. J. Impact, Engng.*1, 393 (1983).
21. J.F. Adie and J.M. Alexander, *Int. J. Mech. Sci.*9, 349 (1967).

Table 1.

TEST NUMBER ACCORDING TO REF.[3]	PROJECTILE	MATERIAL TARGET	HOLE DIA. DAVE OR D1/D3 (mm)	PLUG LENCTH C (mm)	WIDTH OF SHERA ZONE e (mm)	VELOCLTY (m/sec)						CONTAT-KURATION (μ sec)			
						MEASURED		COMPUTED(FINAL)					COMPUTED (μ sec)		
						INITIAL V_i	FINAL V_f	REF [3]	REF[18]	REF[20]	THIS REPORT	MEAS-URED (μ sec)	REF.[3]	REF.[20]	THIS REPORT
11.	S.R.	SA-A-6	10.5	5.0	-	850	500-600	453		478	589	26.9	20.6	20.4	18
12.	S.R.	SA-A-8	10.6	6.9	4.5	855	460	318		454	474	36.2	35.5	30.6	27.6
13.	S.R.	SA-B-6.35	10.4	5.3	3.0	854	350-550	400		463	486		23.6	22.9	19.7
14.	S.R.	SA-C-8	10.0	7.0	3.0	855	450-470	351		455	466	27.8	34.2	30.4	27.3
18.	S.R.	AL-6-9.6	8.2/8.6	2.5	-	845	748	702			742		16		15.5
19.	S.R.	AL-6-13.0	8.1/12.1	7.5	3.0	845	712	602			690		30.2		27.6
10.	S.R.	AL-6-19.0	8.1/13.9	12	4.1	836	568-585	406			516		57.2		51
11.	S.A.P.	SA-A-6	10.5	5.0	-	835	550-650	499	660	467	599		19.5	20.8	16.7
12.	S.A.P.	SA-B-6.35	9.8	5.0	-	848	500-600	492	589	476	578		19.9	21.9	17.6
13.	S.A.P.	SA-D-12	9/5.9	5.5*	5.5	855	300-390	418	364		379		42.1		34
14.	T.T.R.	AL-1-1	5.9	0.7	-	387	369	367		329	373		4.6	4.0	4.6
15.	T.T.R.	AL-1-2	6.0	1.4	-	385	346	342			360		9.6		8.7
20.	T.T.R.	AL-6-1	5.8	0.65	-	379	357	355		310	359		4.2	4.2	4.55
21.	T.T.R.	AL-6-2	6.1	1.5	-	399	341	342			348		9.8		
22.	T.T.R.	AL-6-3	6.6	2.0	1.4	397	309	299			324		15.3		
23.	T.T.R.	AL-6-4	7.1	2.5	1.5	389	268	255			276		20.6		
24.	T.T.R.	AL-6-5	7.8	3.5	1.5	401	174	160		243	225		38.1	33.3	31.8
25.	A.R.	AL-1-4	9.05	2.8	1.75	416	355	345			369		18.6		
26.	A.R.	AL-1-5	9.3	3.5	2.1	422	339	331		343	354	32.0	23.8	19.0	23
27.	A.R.	AL-1-6	9.45	4.2	2.8	428	330	317		341	355	19.0	29.4	22.9	26.2
28.	A.R.	AL-6-3	9.6	1.6	1.75	422	349	354		330	360		12.2	12	11.7
29.	A.R.	AL-6-5	10.3	3.6	109	416	291	276		296	298	24.0	27.3	23.2	25.6
30.	A.R.	AL-6-6.35	10.9	5.0	2.0	412	234	208		276	239	35.0	44.7	33.2	38.8

** See ref.[18]*

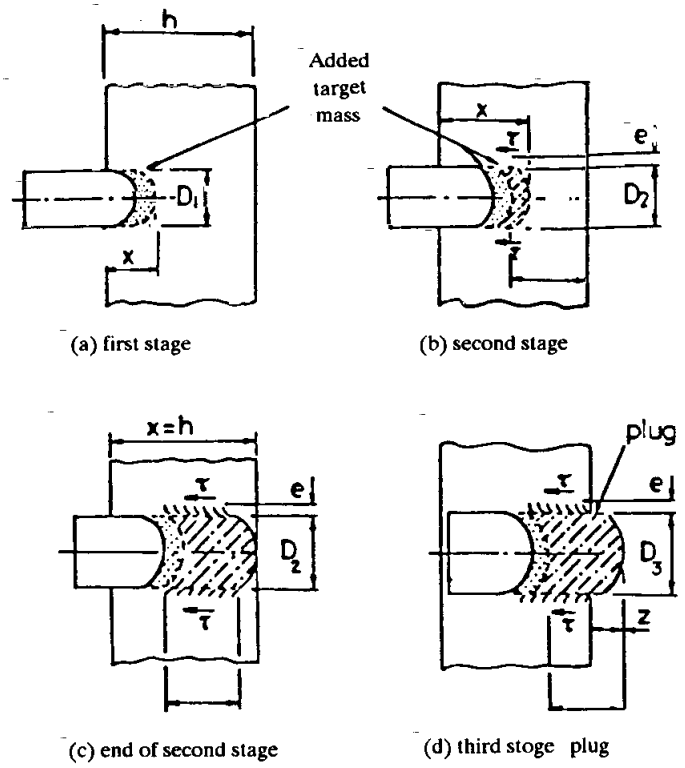

Figure 1. Three stages of the perforation process Awerbuch and Bodner Ref[2] Model.

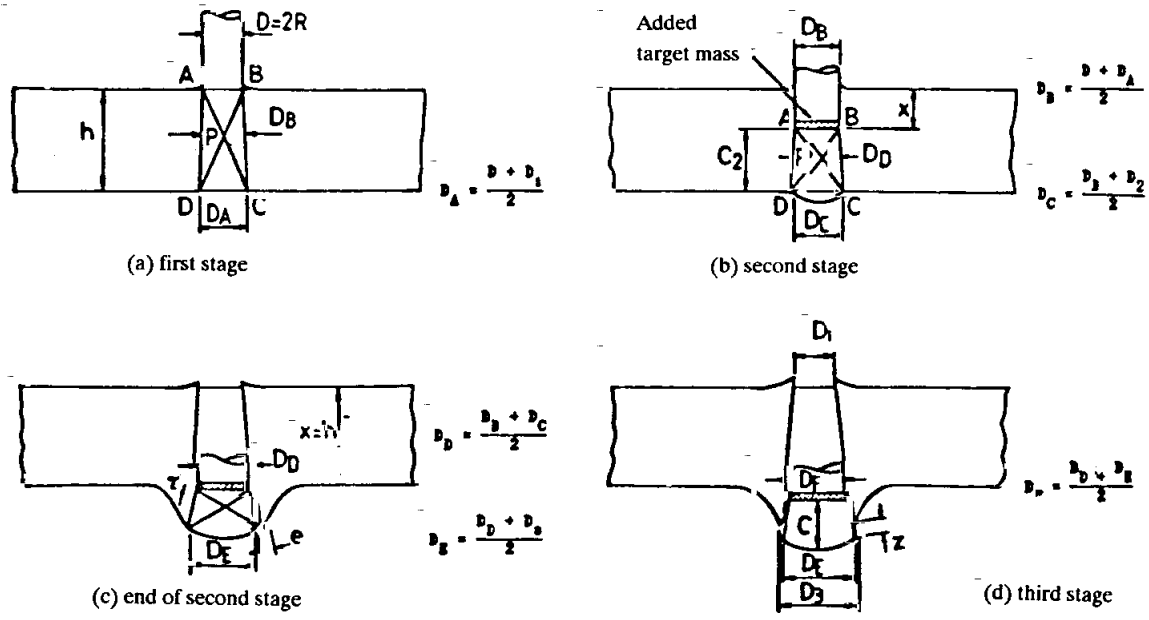

Figure 2. Three stages of the perforation process.

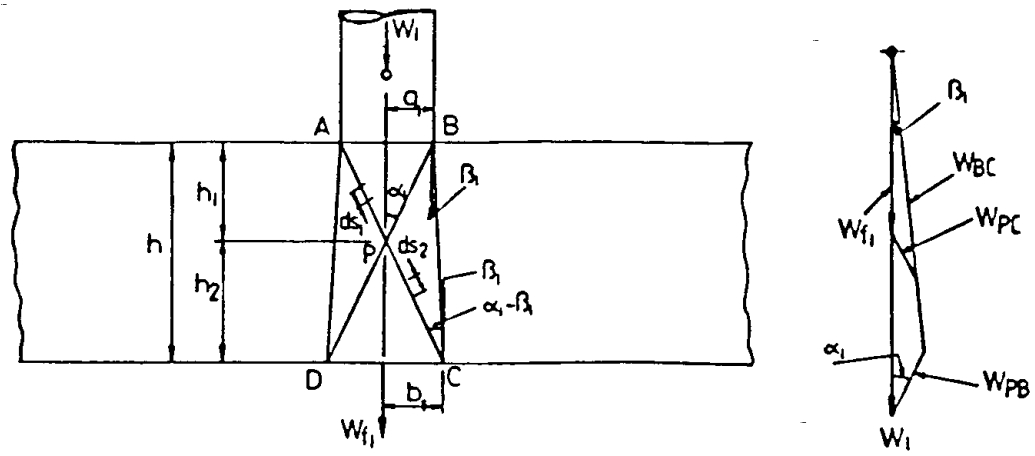

(a) Tangential velocity discontinuty patterns (b) Eodograph

Figure 3. Stoge one of the perforation process and its velocity diogram.

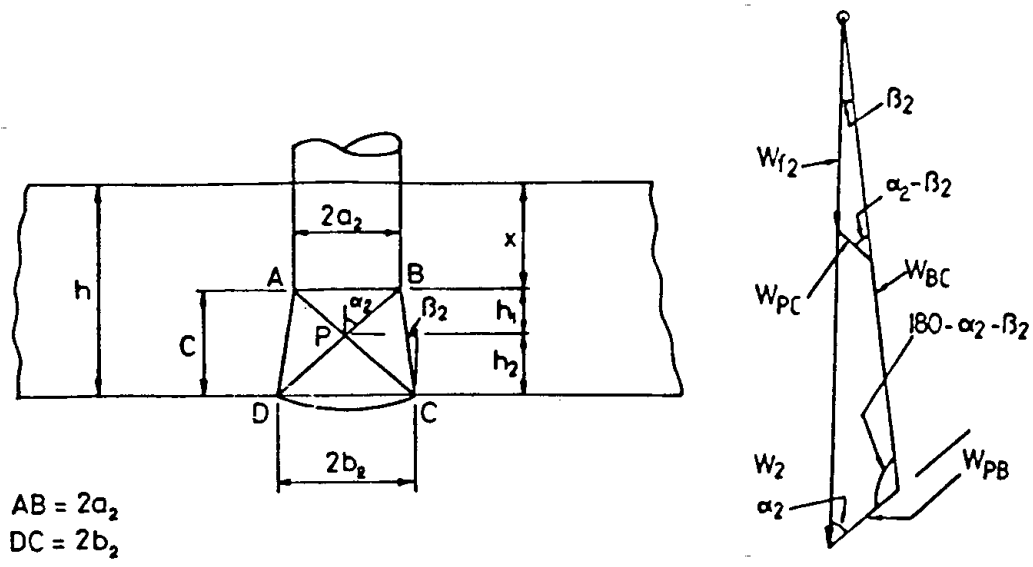

(a) Tangential velocity discontinuty patterns (b) Eodograph

Figure 4. Stage two of the perforation process and its velocity diagram.

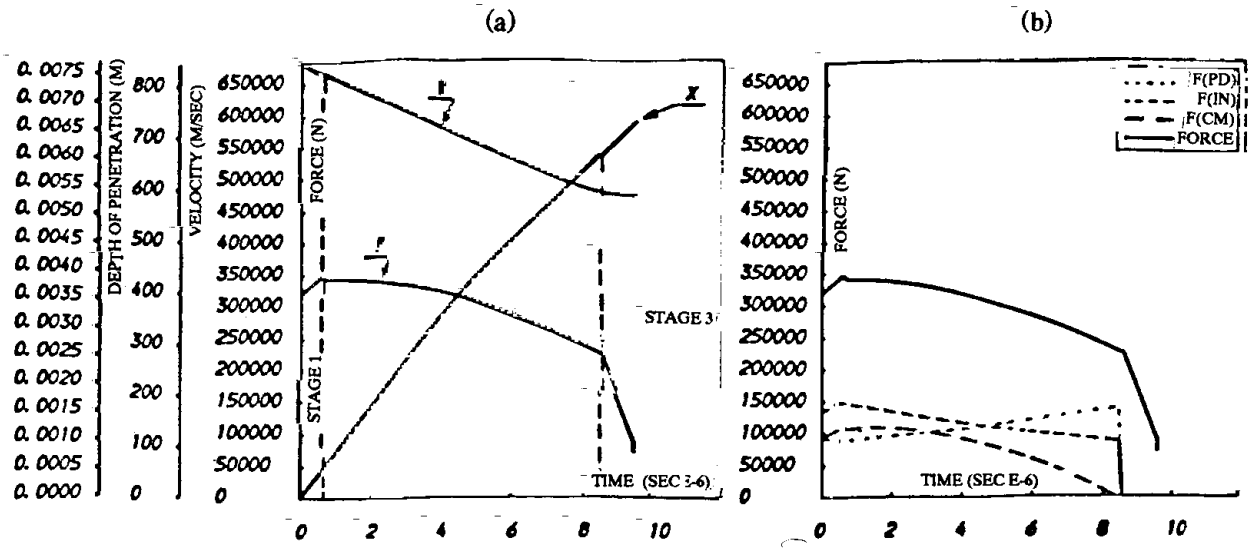

Figure 5. *Test 1.*

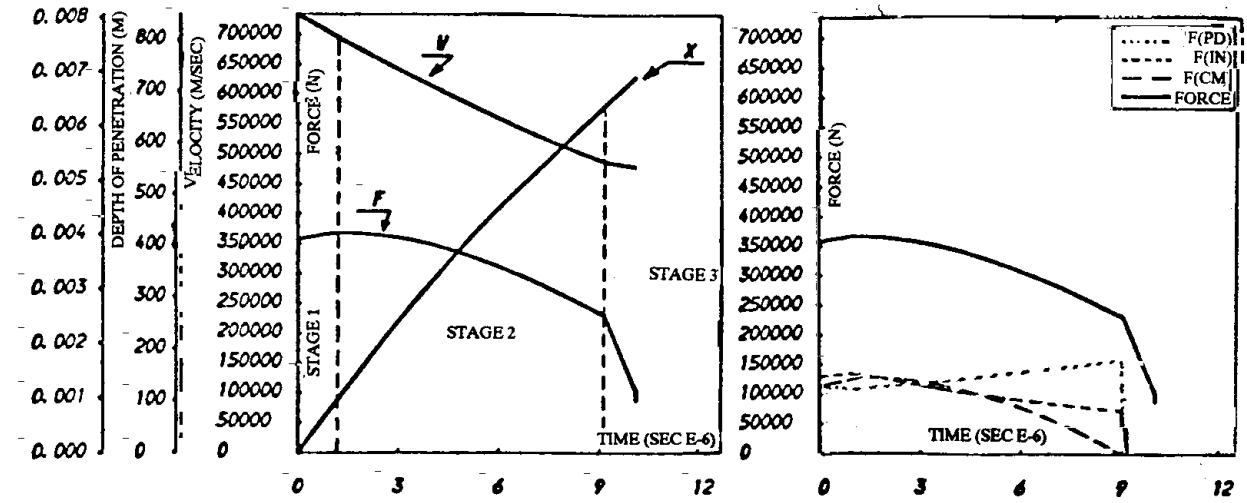

Figure 6. *Test 12.*

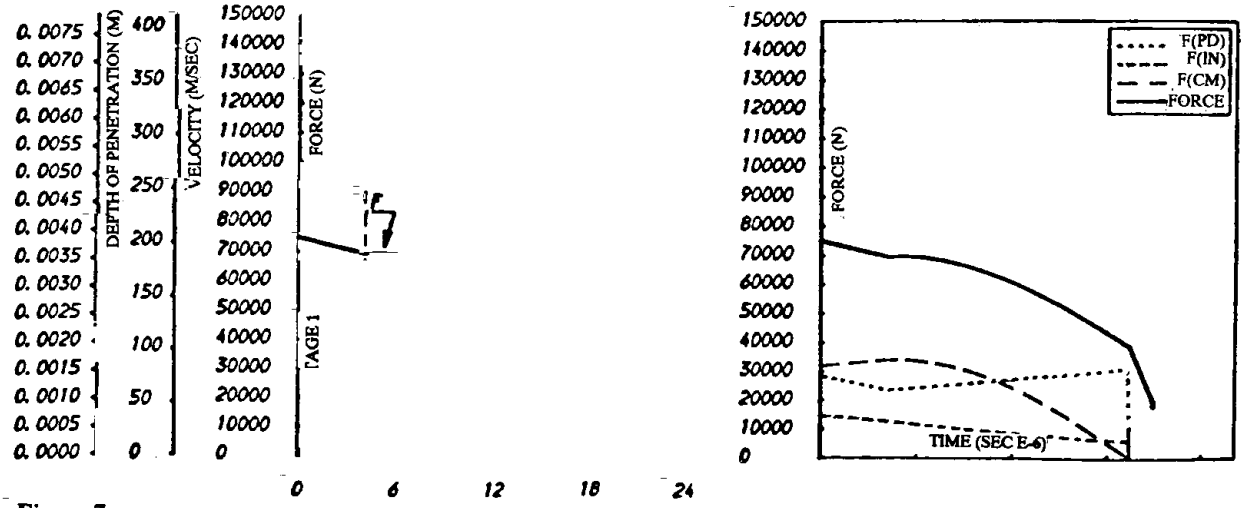

Figure 7.

Computer results of depth of penetration, velocity and force for three stages of perforation process. *Test 30.*